JOURNAL OF MATERIALS SCIENCE 30 (1995) 5923–5926

The effect of retrogression and re-ageing on the ductile fracture toughness of Al-Zn-Mg alloys containing different dispersoid phases

A. UĞUZ*, J. W. MARTIN
Department of Materials, Oxford University Parks Road, Oxford, OX1 3PH, UK

The effects of an incoherent and of a semi-coherent dispersoid phase upon the fracture toughness of a 7000-series AlZnMg alloys has been investigated. Standard crack opening displacement tests were successfully applied, the crack propagation being shown to be predominantly intergranular. The presence of manganese bearing incoherent dispersoids lowers the fracture toughness due to their effect of promoting microvoid formation. Retrogression and re-ageing led to a coarsening of the grain-boundary phases, but because the surface-to-surface separation of these particles remained approximately constant, there was no effect of this treatment, at constant yield stress, upon the fracture toughness. The toughness was only enhanced in the system (CZH) where retrogression and re-ageing led to a reduced yield stress.

1. Introduction

Commercial heat-treatable aluminium alloys contain dispersoids, which are fine particles of intermetallic phases arising from the addition of a transition element such as chromium, manganese, zirconium or vanadium. Their prime function is to control grain growth during heat-treatment, although chromium- and manganese-bearing dispersoids have also been shown to promote homogenization of slip [1, 2]. This effect, together with the refined grain size, increases the tensile ductility and also the fracture toughness [3, 4] of Al–Mg–Si alloys aged to peak hardness. The toughness increases with increasing volume fractions of the incoherent manganese-bearing dispersoid phase. This increase is attributable to the homogenization of slip distribution by the dispersoid phase leading to the blunting of the crack tip.

The present authors have extended these studies to the Al–Zn–Mg system [5], where different micromechanisms of crack extension obtain, in that the crack extends by a predominantly intergranular path during the formation of the stretch zone, so that the crack-tip sharpness is virtually independent of the degree of slip homogenization within the grains. Grain-boundary fracture will be strongly influenced by the distribution of intergranular precipitates, which is likely to be an important microstructural feature relating to the fracture toughness of such alloys. One way of varying the grain-boundary precipitate distribution is by retrogression and re-ageing (RRA), a heat-treatment patented by Cina [6] in order to reduce the susceptibility of the 7000 series aluminium alloys to stress-corrosion cracking (SCC) while still substantially retaining the original strength of the alloy. RRA involves subjecting the peak-aged alloy for a short period at a temperature above that of the ageing, but below that of the solution-treatment temperature. The alloy is then re-aged at the T6 temperature. The beneficial increase in resistance to SCC is believed to be associated with the change in the grain-boundary precipitate distribution during retrogression: their volume, surface area, and spacing will all be changed.

In the present work we have explored the effect of RRA upon the fracture toughness of an Al–Zn–Mg alloy containing a (manganese-bearing) non-coherent dispersoid, a (zirconium-bearing) semi-coherent dispersoid, and a dispersoid-free material.

2. Experimental procedure

The alloys which have been studied are based on the commercial alloy 7005. The principal difference between 7005 and the alloys studied here is the close control of impurity and a lower Zn/Mg ratio (≈ 3.3). The basic alloy composition is 5.5 wt % Zn, 1.7 wt % Mg. A manganese-containing (0.42 wt % Mn) and zirconium-containing alloy (0.15 wt % Zr) have been studied as well as the ternary alloy. In the manganese-containing alloy, silicon was further added to promote the precipitation of $Al_{12}Mn_3Si$ which is an incoherent intermetallic phase. The zirconium-containing alloy forms $ZrAl_3$ which is a body centred tetragonal phase and semi-coherent with the matrix.

The full compositions are given in Table I

For comparative purposes grain size, yield strength and hardness values were kept as close as possible in

Present address: Uludağ University, Mühendislik-Mimarlik Fakültesi, 16059 Görükle, Bursa, Turkey.

0022–2461

TABLE I Compositions of the alloys (wt %)

Alloy code	Zn	Mg	Mn	Zr	Si	Fe	Cu	Al
CTE	5.43	1.71	0.001	—	0.004	0.004	< 0.01	Bal.
CMH	5.47	1.66	0.42	—	0.08	0.007	0.001	Bal.
CZH	5.37	1.64	0.004	0.15	0.01	0.01	0.001	Bal.

TABLE II Summary of tensile and hardness tests with grain sizes

Alloy code	Yield stress (MPa)	UTS (MPa)	Hardness (VDP)	Grain size (μm)
CTE(PA)	389	414	150	105
CTE(RRA)	363	391	139	105
CMH(PA)	388	414	151	101
CMH(RRA)	341	358	142	101
CZH(PA)	394	413	145	80
CZH(RRA)	318	359	130	80

all the three alloys. After recrystallization and solution treatment, all the alloys were naturally aged for 24 h following by peak-ageing (PA) at 130 °C for CTE and CMH, and 120 °C for CZH. After these treatments, a grain size of about 100 μm in CTE and CMH was achieved. However, the grain size of alloy CZH was 80 μm due to zirconium being a powerful grain-growth inhibitor. A yield strength of around 390 MPa was achieved in all three alloys.

After peak-ageing, the three alloys were also subjected to a retrogression and re-ageing (RRA) treatment in order to alter the grain-boundary precipitate distribution. Retrogression ageing was performed at 180° C and re-ageing at the original peak-ageing temperatures until the maximum hardnesses were achieved. A summary of tensile and hardness tests with grain sizes are given in Table II.

2.1. Grain-boundary particle distributions

A detailed TEM analysis of the grain-boundary particle distributions has been conducted, using foils of known thickness, and the results have been reported elsewhere [7]. Average particle sizes, $2r$, and deviations, σ, were calculated and found to vary widely from boundary to boundary, as might be expected, and a boundary triple point illustrating this variation is shown in the thin foil of Fig. 1. The value of σ was smallest where r was smallest, and this effect arises because the smaller particles will tend to be on low-angle grain boundaries, and the larger ones on high-angle boundaries whose higher diffusivity will lead to more rapid particle growth. Direct measurement of the number of particles per unit area of boundary, N_A, was undertaken, and volume fraction, V_f, calculated from the relation

$$V_f = \tfrac{2}{3}\pi r^2 N_A$$

The effect of RRA upon V_f is as shown in Table III.

2.2. Fracture toughness testing

It did not prove possible to conduct standard J_{Ic} tests upon the alloys, because they exhibited pop-in during crack initiation leading to non-reproducible results. Crack opening displacement (COD) tests were successfully carried out according to BS 5762 [8] and the draft method of ASTM e1290-93 [9], employing CT specimens of 6.35 mm thickness machined in the LT direction, i.e. the crack plane was normal to the longitudinal direction. A clip-gauge was attached to the precracked specimen with knife-edges and connected to the strain-gauge amplifier of a screw-driven Instron machine. A crosshead speed of 0.5 mm min^{-1} was employed, and the tests were stopped after pop-in occurred or after some stable crack growth occurred. The measurement of crack length was conducted on a scanning electron microscope (SEM).

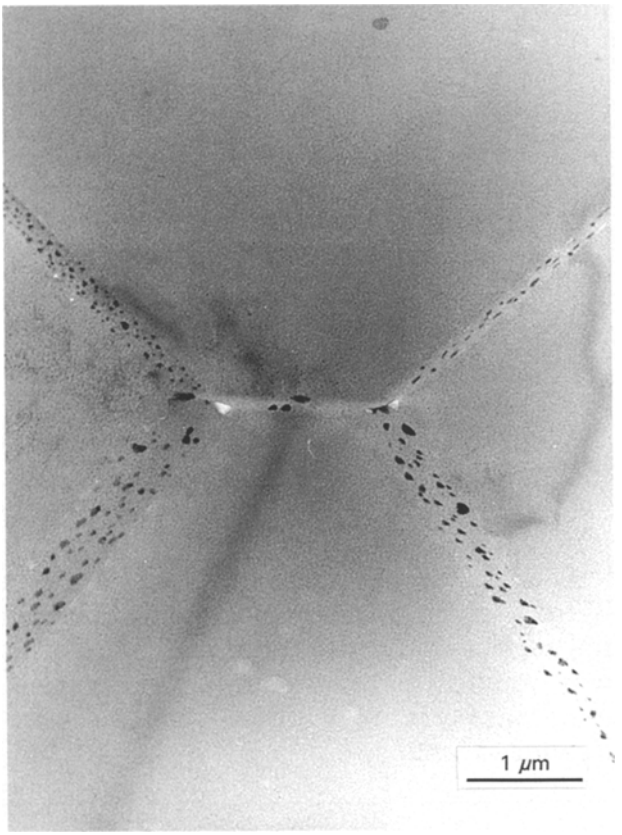

Figure 1 Transmission electron micrograph of CTE showing the variation in size and population of grain-boundary η-phase within a given sample.

TABLE III Volume fraction of grain-boundary particles (%)

Alloy code	CTE	CMH	CZH
PA	1.34%	1.71%	1.41%
RRA	1.92%	2.46%	1.62%

3. Results

3.1. COD measurements

The sum of the elastic and plastic parts of the crack opening was calculated using the relation

$$\delta_t = \frac{K_I^2 (1 - \nu^2)}{2\sigma_{ys} E} + \frac{0.4\ (W - a)\ V_p}{0.4W + 0.6a + Z} \quad (1)$$

where K_I is the applied stress intensity, v is Poisson's ratio, σ_{ys} is the yield strength, E is Young's modulus,

W and a are the width and the initial fatigue cracked length of the specimen, V_p is the clipgauge displacement and Z is the distance of the clipgauge location from the specimen surface. J_{Ic} values shown in Table IV were calculated from the relation:

$$J_{Ic} = M\delta_t\sigma_{ys}, \quad (2)$$

with the value of M taken as 1.3 for all the alloys, using a finite element calculation due to Tracy [10]. Although the requirements for the standard K_{Ic} test method were not satisfied, values of K_Q were calculated (i) using the relation

$$K_Q = \left(\frac{\delta_t\sigma_{ys}EM}{1-\nu^2}\right)^{1/2} \quad (3)$$

and also (ii) by the secant line method on the COD graphs. The former are shown in Table IV as K_Q (calc) and the latter as K_Q(meas.), respectively.

3.2. Fractography

SEM examination of the fracture faces of the test-pieces confirmed that the fracture path was predominantly intergranular in all three PA alloys, and was apparently unaffected by RRA. Fig. 2a and b show the fracture surfaces on CTE (PA) and CMH (PA), and Fig. 3, of CMH (PA) at higher magnification, demonstrates that the intergranular facets show clear evidence of microvoid coalescence upon their surface.

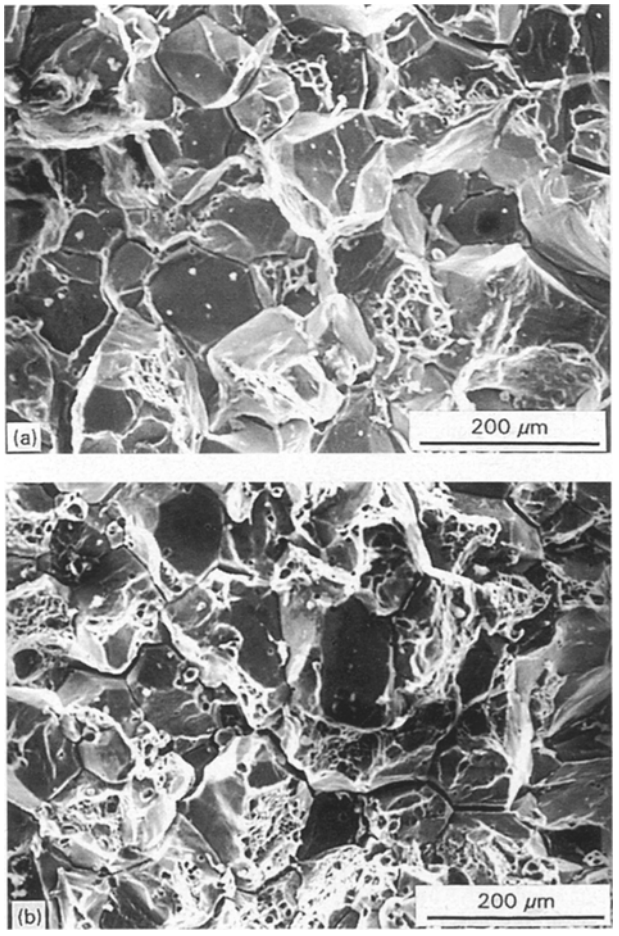

Figure 2 SEM fractograph of (a) CTE, and (b) CMH illustrating the intergranular nature of the fracture.

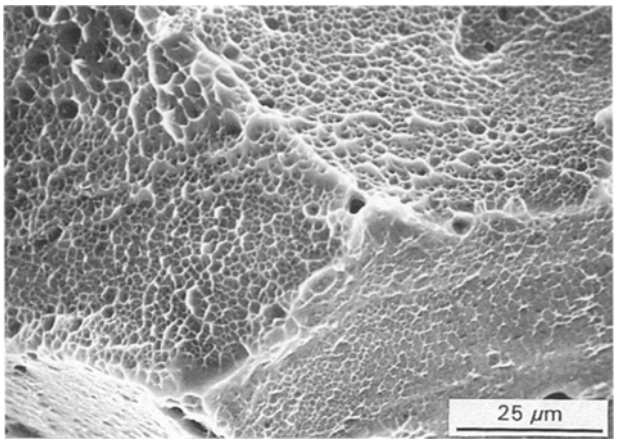

Figure 3 SEM fractograph of CMH at high resolution, illustrating microvoid coalescence over the grain boundary surfaces.

4. Discussion and conclusion

4.1. Peak-aged alloys

It is apparent that the ternary alloy CTE and alloy CZH, which contains the semi-coherent zirconium phase, have closely similar toughnesses. The effect of the non-coherent manganese dispersoid is to bring about a reduction in toughness. This behaviour contrasts with that observed in Al–Mg–Si alloys containing increasing volume fractions of manganese-bearing dispersoids [3] where the particles had the effect of progressively homogenizing the slip distribution, hence increasing the crack-tip radius of curvature and thereby the size of the crack-tip plastic zone. Plastic zone-size measurements on the present alloys as a function of the applied stress intensity [5] revealed that all three alloys obeyed the Rice and Johnson [11] solution, with no apparent slip-distribution effects. Fig. 2 and 3 indicate the predominantly intergranular nature of the crack propagation; it might, therefore, be expected that the crack-tip sharpness would be independent of the degree of slip homogenization, and thus to the presence and type of dispersoid phases.

It is concluded that the significant decrease in toughness in alloy CMH compared with the other two materials arises from the effect, in addition to the incoherent η-phase, of the manganese-bearing dispersoid phases lying in the grain boundaries. Grain-boundary crack propagation is seen (Fig. 3) to be associated with local microvoid coalescence, and Table III reveals that a significantly higher total volume fraction of grain-boundary particles are present in CMH than in the other two alloys. (The grain boundaries would not be preferred sites for the semi-coherent dispersoid in CZH.)

4.2. The effect of RRA

There appears only to be a significant effect of RRA upon the CZH alloy: the origin of this is obvious from the data of Table II, where yield strength after RRA is significantly lowered in this alloy. This implies that there will be less incompatibility between the grain interior and the grain-boundary regions than in the case of the other two alloys, so that there will be less

TABLE IV Summary of fracture toughness data (average of three test results)

Alloy code	COD (μm)	J_{Ic} (calc.) (MPa $m^{1/2}$)	K_Q (calc.) (MPa $m^{1/2}$)	K_Q (meas) (MPa $m^{1/2}$)
CTE(PA)	44.1	22.3	41.9	44.9
CTE(RRA)	45.5	21.5	41.0	43.1
CMH(PA)	35.1	17.7	37.3	41.8
CMH(RRA)	40.2	17.5	37.1	40.4
CZH(PA)	43.7	22.4	41.9	44.2
CZH(RRA)	69.0	28.5	47.3	42.3

tendency for the grain boundaries to open up ahead of the crack tip, and thus a higher toughness will be achieved (Table IV).

It is perhaps more surprising that no significant effect of RRA is found in alloys CTE and CMH. The micromechanism of cracking again involves microvoid coalescence, and the implication of these results is that the grain-boundary particle spacing has not been affected by RRA. The surface-to-surface interparticle spacing of the grain-boundary phases, λ_s^*, may be calculated from

$$\lambda_s^* = (1.2\ N_A^{-1/2}) - 2r \quad (4)$$

and Fig. 4 shows a plot of λ_s^* versus $2r$, where it is seen that there is a sharp increase in λ_s^* with $2r$ (at around a particle size of 65–70 nm). After this point, although the particle size increases, the interparticle spacing appears to remain constant in a narrow band (125–175 nm). In this region large particles grow at the expense of smaller ones, and the surface-to-surface interparticle spacing remains almost constant. It is the particles in the high-angle grain boundaries which are behaving in this way: the small particles will be associated with low-angle grain boundaries because of their impaired diffusivity. During COD testing it will be the high-angle boundaries along which the cracks propagate, as the work needed to propagate along them will be less than along low-angle boundaries. The implication of this rather unexpected constancy of particle spacing is a corresponding constancy of fracture toughness, as has been observed.

We may therefore draw the following conclusions from this study.

1. This alloy system does not permit toughness measurement by means of the standard J_{Ic} test method, because it exhibits pop-in during crack initiation.

2. Standard COD tests have been successfully applied, using standard CT specimens, as suggested by the relevant ASTM standard [9].

3. In COD testing, the starting crack extends intergranularly during the formation of the stretch zone, and the crack sharpness is thus independent of the degree of slip homogenization within the grains.

4. In the peak-aged condition, the manganese-bearing alloy (CMH) exhibits the lowest fracture toughness: this is attributable to the incoherent dispersoid phase promoting microvoid formation.

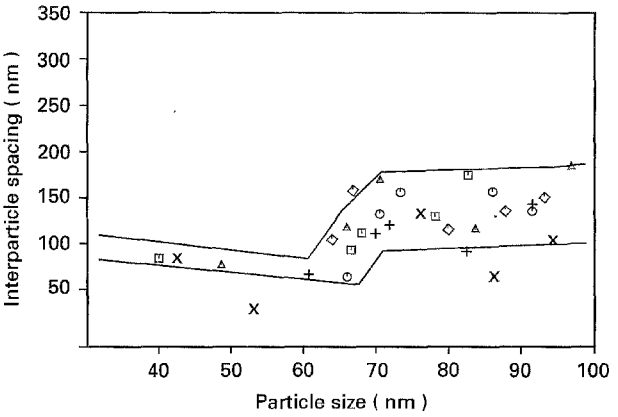

Figure 4 The relation between the particle size and the surface-to-surface interparticle spacings. PA: (□) CTE, (○) CMH, (△) CZH. RRA: (+) CTE, (X) CMH, CZH.

5. The effect of RRA is to enhance the toughness of CZH through the decrease in yield stress. No effect is detectable in CTE or CMH, because the growth in grain-boundary particles is not accompanied by a change in their surface-to-surface separation.

Acknowledgements

The authors are grateful to Professor David Pettifor FRS for the provision of laboratory facilities. Financial support is gratefully acknowledged from Alcan International Ltd, and the Turkish Ministry of Education.

References

1. G. LUTJERING, H. DOKER and D. MUNTZ, in "Proceedings of the 3rd International Conference on Strength of Metals and Alloys", Cambridge, (The Institute of Metals, London, 1973) pp. 427–431.
2. J. M. DOWLING and J. W. MARTIN, *Acta Metall.* **24** (1976) 1147.
3. J. A. BLIND and J. W. MARTIN, *Mater. Sci. Eng.* **57** (1983) 49.
4. A. K. BUSBY, L. EDWARDS and J. W. MARTIN, *Mater. Sci. Technol.* **2** (1986) 363.
5. A. UGUZ and J. W. MARTIN, in "Proceedings of ICF7", Vol. II, edited by K. Salama, K. Ravi-Chandar, D.M.R. Taplin and P. Rama Rao, (Pergamon Press, Oxford, 1989) pp. 1045–52.
6. B. CINA, US PAT. 3856 584, 24 December 1974.
7. A. UGUZ and J. W. MARTIN, *Mater. Charact.* **27** (1991) 147.
8. British Standard BS5762 (British Standards Institute, London, 1979).
9. "Annual Book of ASTM Standards" (American Society for Testing and Materials, Vol. 03.01 Philadelphia, 1993) pp. 952–61.
10. D. M. TRACEY, *Trans. ASME, J. Eng. Mater. Technol.* **98** (1976) 146.
11. J. R. RICE and M. A. JOHNSON, in "Inelastic behaviour of solids" edited by Kanninen, W. F. Adler, A. R. Rosenfield and R. I. Jaffee (McGraw-Hill, New York, 1970) pp. 641–72.

Received 1 May
and accepted 7 June 1995